Journal of Physics: Conference Series

Theoretical spectroscopy of O 1s and N 1s excited states of N_2O

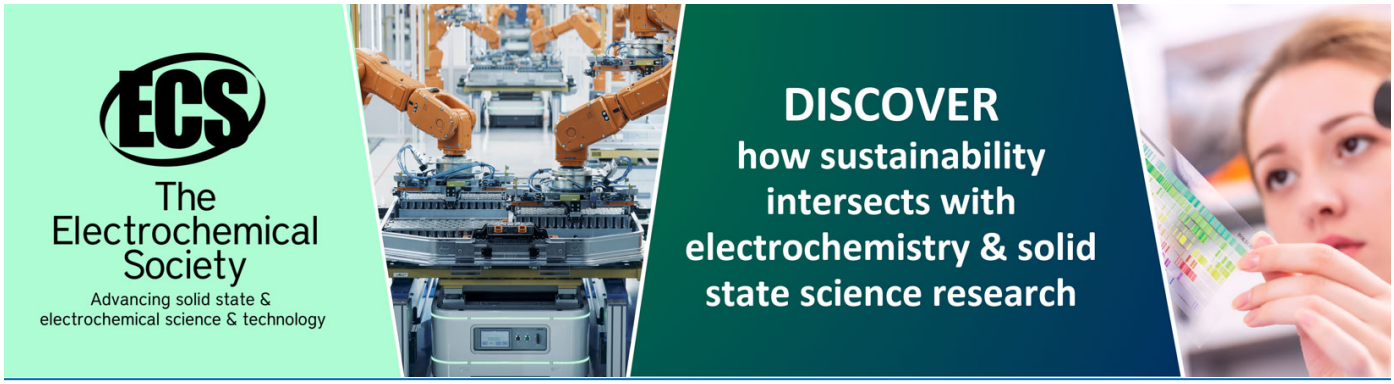

Journal of Physics: Conference Series **288** (2011) 012024 doi:10.1088/1742-6596/288/1/012024

Theoretical spectroscopy of O 1s and N 1s excited states of N_2O

M. Ehara[1,2,3,4*], T. Horikawa[3], R. Fukuda[1,2,4], H. Nakatsuji[4,5], T. Tanaka[6], M. Hoshino[6], H. Tanaka[6], K. Ueda[7]

[1] Institute for Molecular Science, 38 Nishigonaka, Myodaiji, Okazaki 444-8585, Japan
[2] Research Center for Computational Science, Okazaki 444-8585, Japan
[3] Graduate University for Advanced Studies, Okazaki 444-8585, Japan
[4] JST, CREST, Sanboncho-5, Chiyoda-ku, Tokyo 102-0075, Japan
[5] Quantum Chemistry Research Institute, Goryo Oohara 1-36, Nishikyo-ku, Kyoto 615-8245, Japan
[6] Department of Physics, Sophia University,Tokyo 102-8554, Japan
[7] Institute of Multidisciplinary Research for Advanced Materials, Tohoku University, Sendai 980-8577, Japan

E-mail: ehara@ims.ac.jp

Abstract. The O 1s and N 1s excited states of N_2O (nitrous oxide, N_t–N_c–O) have been investigated by the symmetry-adapted cluster–configuration interaction (SAC–CI) method. Our approach in this series of works using high-resolution angle-resolved ion-yield (ARIY) spectroscopy and the SAC–CI method is reviewed for the O 1s excited states of N_2O. The vibrational structure observed by ARIY spectroscopy was interpreted by two-dimensional *ab initio* potential energy surfaces (2D PESs). The valence–Rydberg coupling was analyzed by the electronic part of the second moment, $\langle r^2 \rangle$. The thermal effect in the core-electron excitation spectrum was examined by the PES calculations in the bending coordinate. The 2D PESs of the N_t and N_c excited states have also been calculated by the SAC–CI method and are discussed in detail.

1. Introduction

Molecules show the characteristic geometry changes by the core-electron excitations/ionizations, which originates from the significant orbital relaxation in the core-electron processes [1]. This characteristic geometry changes can be observed in the vibrational spectra by photoexcitation spectroscopy. Recently, much effort has been devoted to probing the geometry changes and dynamics by experiment [2]. To interpret these spectra and excited-state dynamics, however, accurate theoretical information on the molecular structure in the core-excited and ionized states is indispensable.

Recent state-of-the-art theories has enabled us to obtain precise knowledge of the core-electron excited or ionized states. Theoretical information is valuable in interpreting the wide variety of the high-resolution spectra. Theory predicts the fine details of the excitation and ionization processes. Therefore the interplay between experiment and theory has become important in modern molecular spectroscopy so that the predictive ability of a theory is an essential issue.

The vibrational spectra and geometry relaxation of the O 1s and N 1s excited states of N_2O (nitrous oxide) are of interest because the vibrational spectra in these states show different features. N_2O has two nonequivalent nitrogen atoms, the terminal N_t and the center N_c, and therefore, the chemical environment in these core-excited states is different. Adachi et al. [3] presented the first angle-resolved energetic-ion yield (ARIY) spectra of the N 1s and O 1s excited states of N_2O, and investigated them with *ab initio* SCF calculations. They paid special attention to the O $1s^{-1}$ π^*, N_c $1s^{-1}$ π^*, and N_t $1s^{-1}$ π^* excitations and showed that the Renner–Teller coupling via the (0, ν_2', 0) mode breaks the degeneracy of these Π states. Tanaka et al. [4] found that the Renner–Teller effect in these Π states is pronounced in a hot target molecule. Adachi further showed that no Renner–Teller effect is present in any of the Rydberg excited states. Prince et al. [5] reported total yield X-ray absorption fine structure spectra without symmetry resolution, but at high energy resolution near both the N 1s and O 1s edges of N_2O several new Rydberg states were found in their study. Thus, these spectra have been well investigated; however, for the detailed assignments and interpretation of the spectra, reliable theoretical calculations including electron correlation are still necessary. In particular, information on the potential energy surfaces (PESs) is relevant to understanding the vibrational spectra and geometry changes in the O 1s and N 1s excited states of N_2O. The geometry changes in these core-excited states can be qualitatively understood by the electrostatic force theory [6,7].

Theoretical spectroscopy on the core-electron states has been achieved by various types of electronic structure theories. Peyerimhoff and co-workers performed pioneering work using the multireference single and double configuration interaction (MRSDCI) method [8,9]. Cederbaum and co-workers have greatly contributed to the inner-shell electronic processes as well as the valence ionizations using the Green's function method called the algebraic diagrammatic construction (ADC) approach [10,11]. They introduced essential and useful chemical concepts for those electronic processes, which have accelerated the development of this field. Theories based on cluster expansion have also been applied to the core-electron processes such as the symmetry-adapted cluster–configuration interaction (SAC–CI) method originally developed by Nakatsuji [12,13] and the multireference coupled cluster method proposed by Jana and Mukherjee [14]. Recently, time-dependent density functional theories (TDDFT) with new functionals designed for the core-electron processes have also been developed [15].

The SAC–CI method [12,13] has been successfully applied to a wide range of chemistry and physics. The method has been established as a useful tool for investigating molecular excited states through numerous applications to molecular spectroscopy, biological chemistry, and surface chemistry [16,17]. The SAC–CI general-*R* method [18,19] is designed to investigate the complex multielectron processes such as shake-up satellite states and has been successfully applied to those processes [17]. Because the method is applicable to general electronic states, it provides a powerful tool for the inner-shell electronic processes. The SAC–CI method with the equivalent core model (ECM) is also useful for studying the vibrational structure and geometry relaxation in the core-electron states. There, we can use the SD-*R* method in the direct SAC–CI framework [20]. We have investigated various types of core-electron processes with the SAC–CI method [21-29]; for example, core-electron binding energies, inner-shell shake-up satellite spectra, vibrational spectra and geometry relaxation of satellites, g–u splitting, valence–Rydberg coupling, and its vibration-induced suppression.

In this article, we review our recent experimental and theoretical work on the O 1s excited states of N_2O [28] and present a SAC–CI study on the N 1s excited states; namely, the two-dimensional potential energy surfaces (2D PESs) of the N_t 1s and N_c 1s excited states with regard to π^*, $n\mathrm{p}\pi$ (n = 3–5), $n\mathrm{s}\sigma$ (n = 3–5), and $n\mathrm{p}\sigma$ (n = 3, 4) transitions.

2. Theory

2.1. SAC/SAC–CI theory

The 2D PESs of the ground, O 1s excited, and N 1s excited states were calculated along the direction of the normal coordinates q_1 and q_3 corresponding to the quasisymmetric (ν_1') and quasi-antisymmetric (ν_3') stretching vibrational motions, respectively, in the ranges R_{NN} = 1.00−1.30 Å and R_{NO} = 1.00−1.55 Å. The basis sets were the correlation-consistent polarized valence triple zeta (cc-pVTZ) basis sets proposed by Dunning without f function, namely [4s3p2d] [30] plus Rydberg functions [5s5p] [31] placed on the central N atom for describing n = 3, 4, 5 (s, p, and d functions for O 1s excited states, and s and p functions for N 1s excited states).

The ground and core-excited states of N_2O were calculated by the SAC and SAC–CI methods, respectively. The ground-state geometry was calculated to be R_{NN} = 1.122 and R_{NO} = 1.184 Å, in good agreement with the experimental values [32] of 1.127 and 1.185 Å, respectively. To calculate the 2D PESs of the core-excited states, the ECM was adopted. For the O 1s, N_t 1s, and N_c 1s excited states, the excited states of NNF, ONO, and NOO molecules, respectively, were calculated by the SAC–CI method. SAC–CI SD-R calculations in which single (S) and double (D) excitations were adopted for the R-operators were performed and the excited states of the neutral radicals ONO and NOO were calculated by electron attachment to ONO^+ and NOO^+, respectively. We employed the algorithm calculating σ-vectors directly that includes all of the S_2R_1 and S_2R_2 nonlinear terms [20]. All of the S- and R-operators were included without perturbation selection in the SAC–CI calculations. The equilibrium geometries of each state were obtained by the analytical energy gradients of the SAC–CI method. The optimized structures were confirmed to be local minima by calculating the PESs in the bending coordinate.

The SAC–CI calculations were performed with the development version of the Gaussian09 suite of programs [33].

2.2. 2D vibrational analysis

The vibrational analysis was performed using the SAC–CI 2D PESs of the O 1s and N 1s excited states of N_2O. To calculate the Franck–Condon (FC) factors of the vibrational spectrum, the vibrational wave function was obtained by the grid method, in which the Lanczos algorithm was adopted for the diagonalization. The 2D PESs of the N_2O molecule were described in the bonding coordinates where the bond distances are r_1 and r_2, the bond angle being fixed. In this coordinate, the kinetic part of the Hamiltonian of the vibrational motion is given by:

$$T = \frac{p_1^2}{2\mu_{N_cN_t}} + \frac{p_2^2}{2\mu_{N_cO}} + \frac{p_1 p_2}{m_{N_c}},\ p_k = -i\frac{\partial}{\partial r_k},\ k = 1,2,$$

and $\mu_{N_cN_t}$ is the reduced mass of N_t and N_c atoms. The coordinates r_1 and r_2 are represented by the Hermite discrete variable representation [34]. The 2D PESs were fitted by the analytical functions of the 2D Morse expansion:

$$V(r_1, r_2) = \sum_{i,j=0}^{n} B_{ij}(1 - e^{-a_1(r_1 - r_{e_1})})^i (1 - e^{-a_2(r_2 - r_{e_2})})^j,$$

where r_{e_1} and r_{e_2} are equilibrium distances and are determined by the analytical energy gradients of the SAC/SAC–CI method. This function is suitable for describing the PESs of the bound state [35]. The vibrational spectra were calculated in the framework of the FC approximation. These calculations were conducted using the MCTDH program system developed by the Heidelberg group [36].

3. Applications to core-electronic processes

3.1. O 1s excited states of N_2O

ARIY spectra were measured in the O K edge of N_2O [28]. Figure 1 shows the ARIY spectra measured at angles of 0° and 90° relative to the polarization vector along with the total ion yield measurement. The measurement at 0°, ARIY(I(0°)), mainly observes the Σ states, while the

measurement at 90°, ARIY(I(90°)), observes the Π states. In the ARIY(I(0°)), the Σ and Π states interfere with each other; therefore, the Σ spectrum cannot be resolved completely. In the O $1s^{-1}$ 4sσ state, irregular excitation to the higher vibrational levels was observed, while the vibrational spectrum of the 3pπ state was a normal Rydberg spectrum.

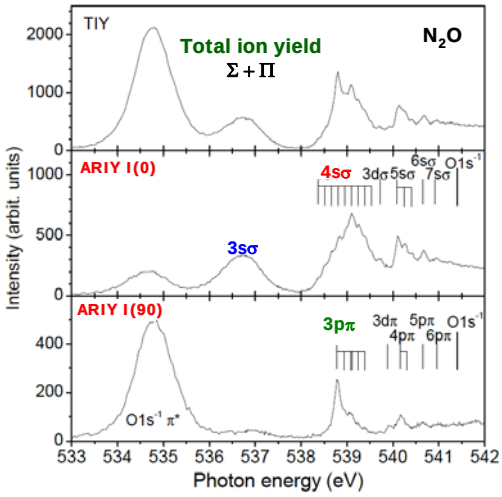

Figure 1. ARIY spectra of O 1s excitation of N_2O measured at 0° and 90° relative to the polarization vector [28].

To clarify this irregular vibrational progression, the PESs of the O 1s core-excited states were examined [28]. Figure 2 show the PESs and the electronic part of the second moments $\langle r^2 \rangle$ of the O 1s excited states of Σ and Δ symmetry along the R_{NO} distance. The second moment $\langle r^2 \rangle$ of the Rydberg states increases monotonically with R_{NO}, while that of the O $1s^{-1}$ 4sσ state decreases drastically at large R_{NO}. This shows that strong valence–Rydberg coupling occurs in the O $1s^{-1}$ 4sσ state having a σ* component. Because of this strong valence–Rydberg coupling, the O $1s^{-1}$ 4sσ state has a potential energy minimum at large R_{NO}. This shows that the irregular Rydberg behavior in the O $1s^{-1}$ 4sσ state is caused by the strong valence–Rydberg coupling.

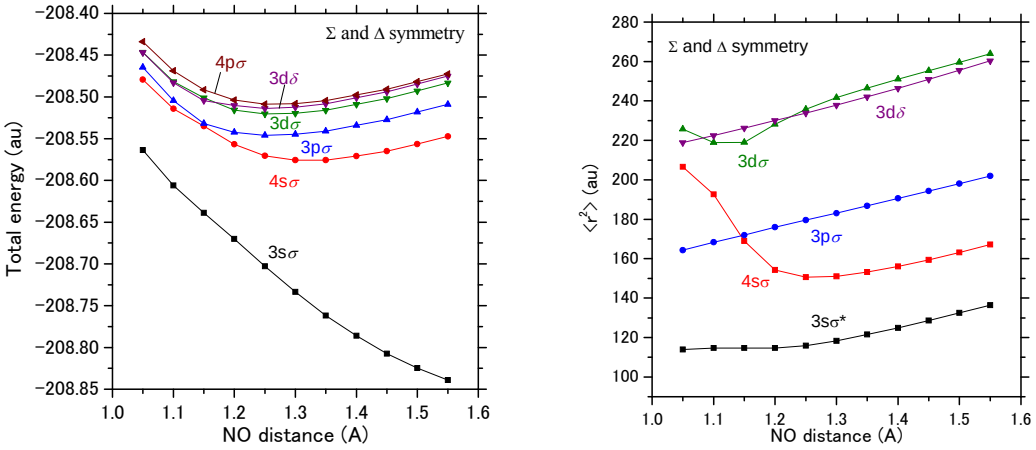

Figure 2. Potential energy curves (left) and second moments $\langle r^2 \rangle$ (right) of the O 1s excited states of N_2O [28].

The FC analysis based on the SAC–CI 2D PESs was performed for the O $1s^{-1}$ 4sσ and 3pπ states [28]. In Figure 3, theoretical spectra are compared with the ARIY $I(0°)$ and $I(90°)$ spectra for the O $1s^{-1}$ 4sσ and 3pπ states, respectively. Theory reproduced the observed vibrational excitations accurately. The higher vibrational levels are excited in the O $1s^{-1}$ 4sσ state, while the vibrational spectrum of the 3pπ state shows the standard Rydberg-type vibrational progression.

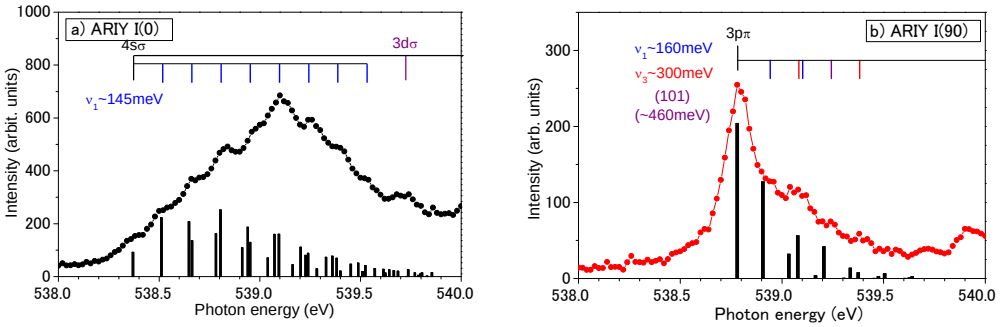

Figure 3. Vibrational spectra of a) O $1s^{-1}$ 4sσ (ARIY, $I(0°)$) and b) O $1s^{-1}$ 3pπ (ARIY, $I(90°)$) excited states of N_2O. The SAC–CI spectra are shown by the vertical solid lines [28].

3.2. Thermal effects in core-electron excitation spectra

Absorption spectra of vibrationally excited "hot" molecules were observed for the O 1s excitation of N_2O [29]. The absorption spectra were measured at 300/700 K and the vibrationally excited absorption spectrum was extracted assuming the Boltzmann distribution (Figure 4) [29]. Based on the Boltzmann distribution, the bending mode is dominantly excited in the ground state. Comparing the spectra of (0, 0, 0) and (0, v_2, 0), the intensity of the *n*sσ Rydberg series is significantly suppressed and the peaks show a blue shift. The absorption of the $A'(\pi)$ state, on the other hand, is enhanced for the excitation from the vibrationally excited states, (0, v_2, 0), and shows a red shift. These observations suggest that the decrease in the bond angle causes a decrease in the mixing of the valence character that enhances the transition probability to the Rydberg states.

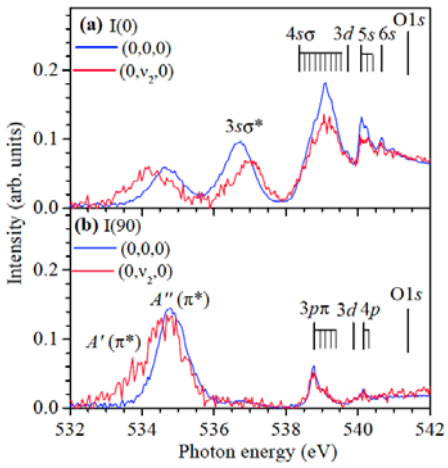

Figure 4. ARIY spectra in the N_2O O 1s excitation region: blue and red lines show the spectra from the vibrational ground and excited states, respectively [29].

To understand these phenomena, we performed SAC–CI calculations of the energies and the second moments $\langle r^2 \rangle$ of the O 1s excited states varying the bond angle [29]. Figure 5 shows a cut of the calculated PESs of the O 1s excited states of A' symmetry. The $1A'$ state is correlated with the π*

state and stabilizes along the bending coordinate. All of the other states are stable in the linear structure. A characteristic curve crossing occurs between the σ and π Rydberg states along the bending coordinate. These PESs explain the red shift of the π* state and the blue shift of the 3sσ and 4sσ states. To analyze the valence–Rydberg coupling, we examined the electronic part of the second moment $\langle r^2 \rangle$, which is anticorrelated with the amount of valence character (Figure 5). The second moment of the 3sσ, 4sσ, and 5sσ states becomes larger as the molecule becomes more bent. This indicates that the mixing of the valence character in these states becomes less as the bond angle decreases. Consequently, the absorption intensity of the *n*sσ Rydberg states weakens. These results explain the interpretation of the intensity changes observed for excitation from vibrationally excited molecules.

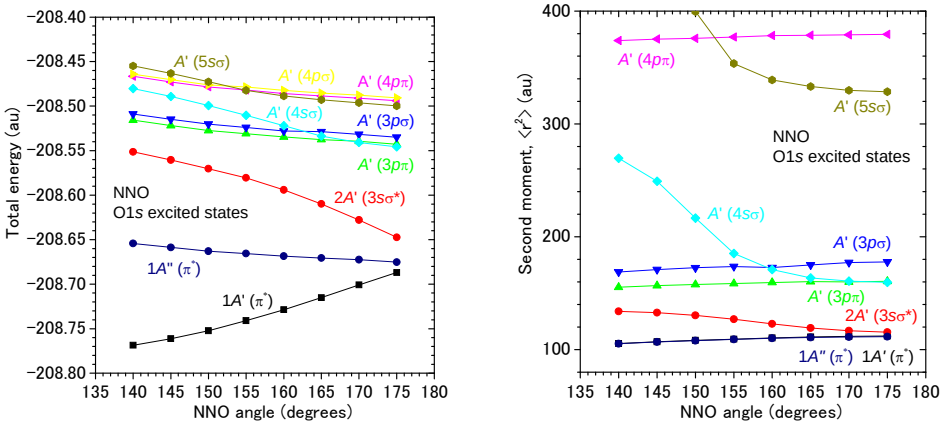

Figure 5. Potential energy curves (left) and second moments $\langle r^2 \rangle$ (right) of the low-lying O 1s excited states of N_2O along the bending coordinate [29].

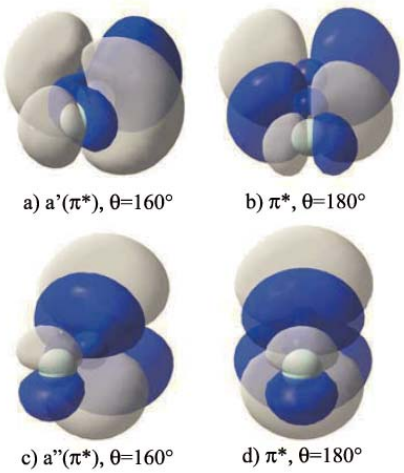

Figure 6. Calculated in-plane $a'(\pi^*)$ and out-of-plane $a''(\pi^*)$ MOs at bond angles of θ=160° and 180°[29].

The $A'(\pi^*)$ state stabilizes along the bending coordinate whereas the 3sA' state destabilizes more than the $A''(\pi^*)$ state. This anticorrelation indicates that the $A'(\pi^*)$ and 3sA' states are strongly coupled. This coupling opens a flow of valence character from the 3sA', 4sA', and 5sA' Rydberg states to the $A'(\pi^*)$ state. Analyzing the MOs that contribute to the excitations, we conclude that the counterpart of the decrease in the mixing of the valence character in the 3s, 4s, and 5s states is an increase in the sσ-type character of the $a'(\pi^*)$ orbital. The π* MO is displayed in Figure 6. Figures 6(c) and 6(d) show that the out-of-plane $a''(\pi^*)$ MO has a pure pπ-type orbital independent of bond angle. For the in-plane

a'(π*) MO, on the other hand, the sσ-type orbital component contributes to the MO, as can be seen in Figures 6(a) and 6(b).

Based on the SAC–CI calculations of the second moment $\langle r^2 \rangle$, the suppression is interpreted as being the result of a decrease in the mixing of the valence character in the *n*sσ Rydberg states with decreasing bond angle.

3.3. N_t 1s excited states of N_2O

The ARIY spectra of the N 1s excited states of N_2O were also observed in the energy range 399–413 eV. The ARIY spectra and its theoretical interpretations are presented in a separate note [37]. In this article, we discuss the results of the 2D PESs of the N_t 1s and N_c 1s excited states regarding the π*, *n*pπ (*n* = 3–5), *n*sσ (*n* = 3–5), and *n*pσ (*n* = 3, 4) transitions. We also compare those PESs with the PESs of the O 1s excited states.

The 2D PESs of the N_t 1s excited states were investigated by the SAC–CI method within the ECM approximation. Figures 7 and 8 show the 2D PESs of these states with Π- and Σ-symmetry, respectively, for R_{NN} = 1.00, 1.10, 1.20, and 1.30 Å. The N_t $1s^{-1}$ π* excited state shows a bound state in the N–O distance as in the O $1s^{-1}$ π* excited state. Other *n*pπ Rydberg excited states have almost the same shape for the PESs converging to the N_t $1s^{-1}$ ionized state. The PESs of the N_t $1s^{-1}$ *n*sσ and *n*pσ states show a characteristic shape. In the range R_{NN} = 1.00–1.20 Å, the N_t $1s^{-1}$ 3sσ state has a flat region around the FC region in the PES. For larger internuclear distances $R_{NN} \geq 1.30$ Å, the PES of this state becomes bound. The energy minimum in the N_t $1s^{-1}$ 3sσ state exists for a very large R_{NN} distance. The PESs of the N_t $1s^{-1}$ 4sσ and 3pσ states have an avoided crossing in the region of R_{NN} =

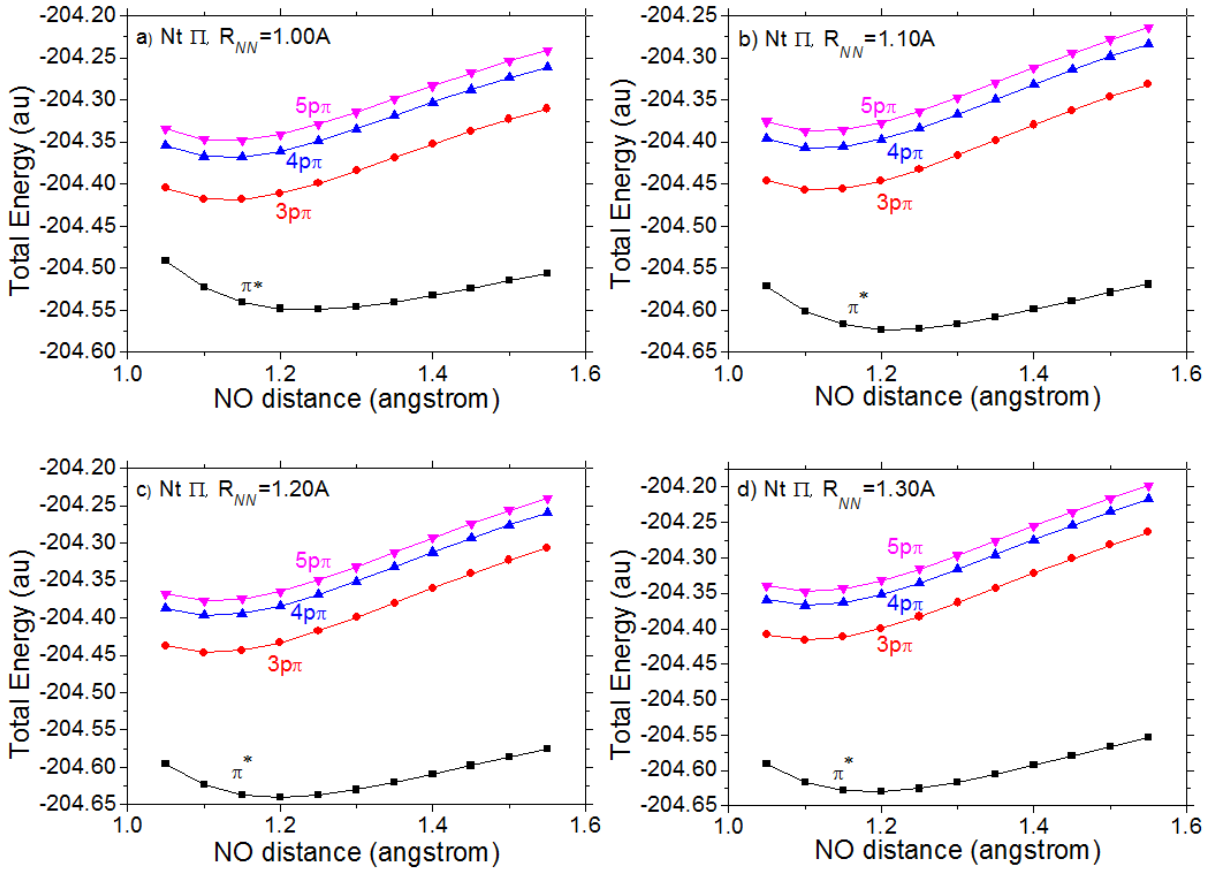

Figure 7. The 2D PESs of the low-lying N_t 1s excited states (π* and *n*pπ (*n* = 3–5) transitions) of N_2O in the R_{NO} coordinate for R_{NN} = 1.00, 1.10 [37], 1.20, and 1.30 Å.

1.00–1.20 Å. The valence–Rydberg coupling of the N_t $1s^{-1}$ 4sσ state, however, is not so large in the FC region, and therefore the 3pσ state is more stable than the 4sσ state. This situation of the N_t $1s^{-1}$ 4sσ state is different from that in the O $1s^{-1}$ 4sσ state shown in Figure 2. For the large internuclear distance of $R_{NN} \geq 1.30$ Å, valence–Rydberg coupling of the N_t $1s^{-1}$ 4sσ state becomes large and its PES is much lower in energy than that of the N_t $1s^{-1}$ 3pσ state. The PESs of the N_t $1s^{-1}$ 5sσ and 4pσ states also interact with each other in the same manner.

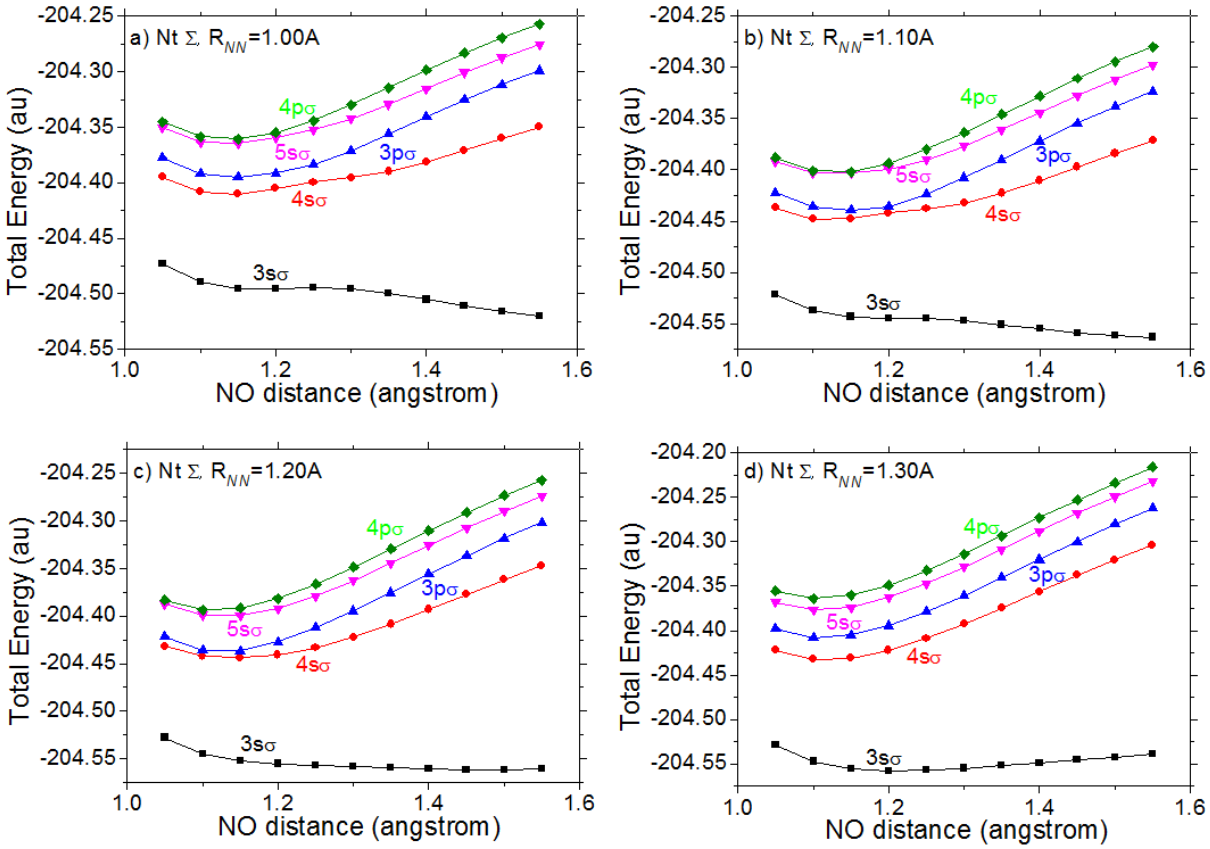

Figure 8. The 2D PESs of the low-lying N_t 1s excited states (*n*sσ (*n* = 3–5) and *n*pσ (*n* = 3, 4) transitions) of N_2O in the R_{NO} coordinate for R_{NN} = 1.00, 1.10 [37], 1.20, and 1.30 Å.

3.4. N_c 1s excited states of N_2O

The 2D PESs of the N_c 1s excited states were also calculated by the SAC–CI method in the same manner. The PESs are shown in Figures 9 and 10 for Π- and Σ-symmetry, respectively, for R_{NN} = 1.00, 1.10, 1.20, and 1.30 Å.

The PES of the N_c $1s^{-1}$ π* excited state is repulsive in the N–O coordinate, which is different from those of the O $1s^{-1}$ π* [28] and N_t $1s^{-1}$ π* excited states. Other *n*pπ Rydberg excited states are bound; however, their PESs are flat in the R_{NO} coordinate compared with the O 1s and N_t 1s Rydberg states. These PESs converge monotonically to the N_c $1s^{-1}$ ionized state. The PESs of the N_c $1s^{-1}$ *n*sσ and *n*pσ states have repulsive character compared with those of the O $1s^{-1}$ and N_t $1s^{-1}$ Rydberg excited states for the *n*sσ and *n*pσ transitions. The N_c $1s^{-1}$ 3sσ state is intrinsically repulsive, while other states are bound, with their equilibrium R_{NO} distances being relatively large. In the range R_{NN} = 1.00–1.20 Å, the PES of the N_c $1s^{-1}$ 4sσ state has an avoided crossing with the N_c $1s^{-1}$ 3pσ state. In the N_c $1s^{-1}$ 4sσ state, valence–Rydberg coupling is strong even in the FC region and the repulsive nature is remarkable. The

valence–Rydberg mixing of other states is not so strong from the nature of their PESs. Therefore, the equilibrium bond length of the N–O bond becomes large. Other higher N_c $1s^{-1}$ nsσ and npσ states are flat. The PESs of the N_c $1s^{-1}$ 5sσ and 4pσ states also interact at small R_{NN} and R_{NO} distances.

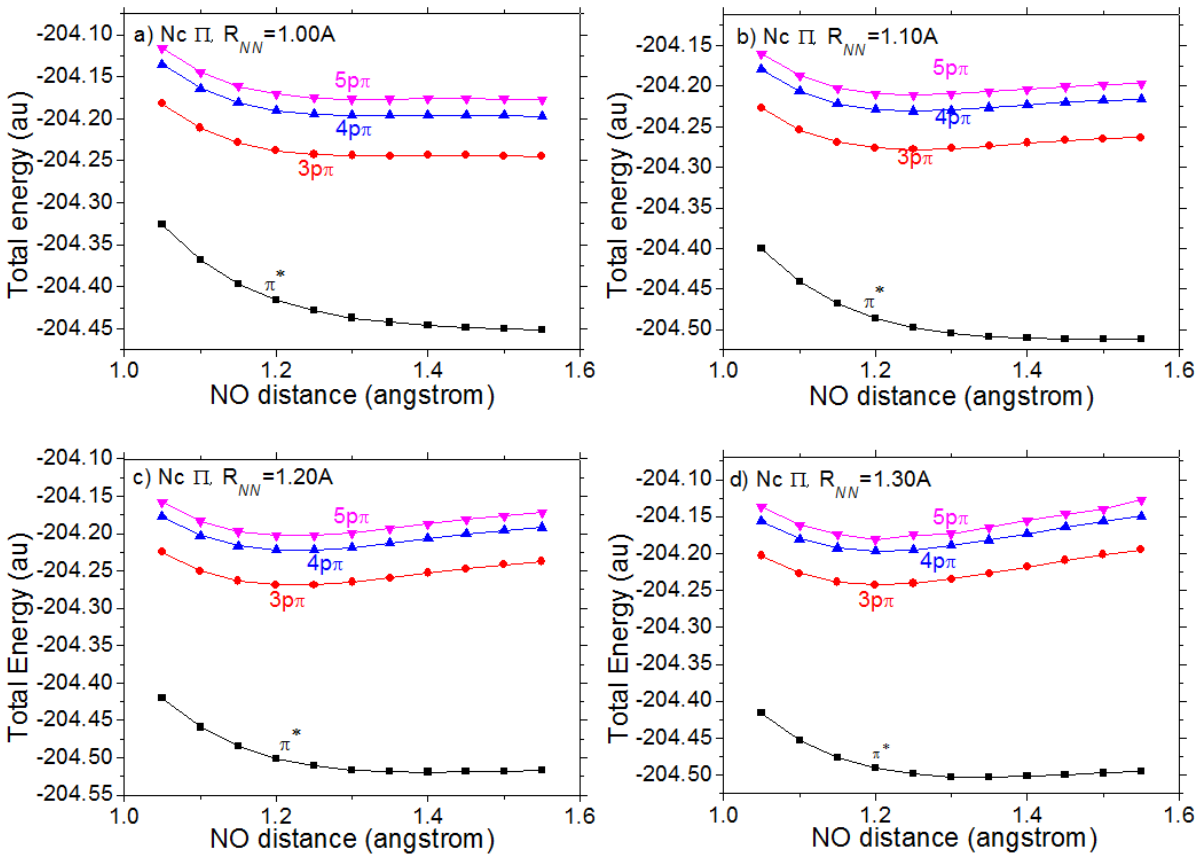

Figure 9. The 2D PESs of the low-lying N_c 1s excited states (π* and npπ (n = 3–5) transitions) of N_2O in the R_{NO} coordinate for R_{NN} = 1.00, 1.10 [37], 1.20, and 1.30 Å.

4. Summary

In this article, we present joint work on the O 1s and N 1s excited states of N_2O using high-resolution ARIY spectroscopy and the SAC–CI method.

The high-resolution ARIY was observed in the region of the O 1s edge of N_2O. The vibrational excitations were found to be specific to the individual Rydberg states in the Σ-symmetry spectrum. The FC analysis based on the SAC–CI 2D PESs well reproduces the observed state-specificity of the vibrational excitations. The irregular vibrational excitations along the same nsσ Rydberg series were attributed to valence–Rydberg coupling.

A significant suppression of the intensity in the O 1s → nsσ Rydberg series in N_2O for excitation from the bending vibrationally excited ground states was observed. Based on the second moment analysis, this suppression was attributed to a decrease in the mixing of the valence character in the nsσ Rydberg states with decreasing bond angle.

The 2D PESs of the low-lying N_t 1s and N_c 1s excited states of N_2O have also been investigated by the SAC–CI method. The bound nature of the PESs of the N_t 1s excited states is strong compared with those of the O 1s excited states, while the PESs of the N_c 1s excited states have a repulsive character.

The valence–Rydberg coupling in the N_c 1s excited states is strong, in particular in the N_c $1s^{-1}$ 3sσ and 4sσ states. Detailed assignments of the ARIY spectra are presented in a separate note [37].

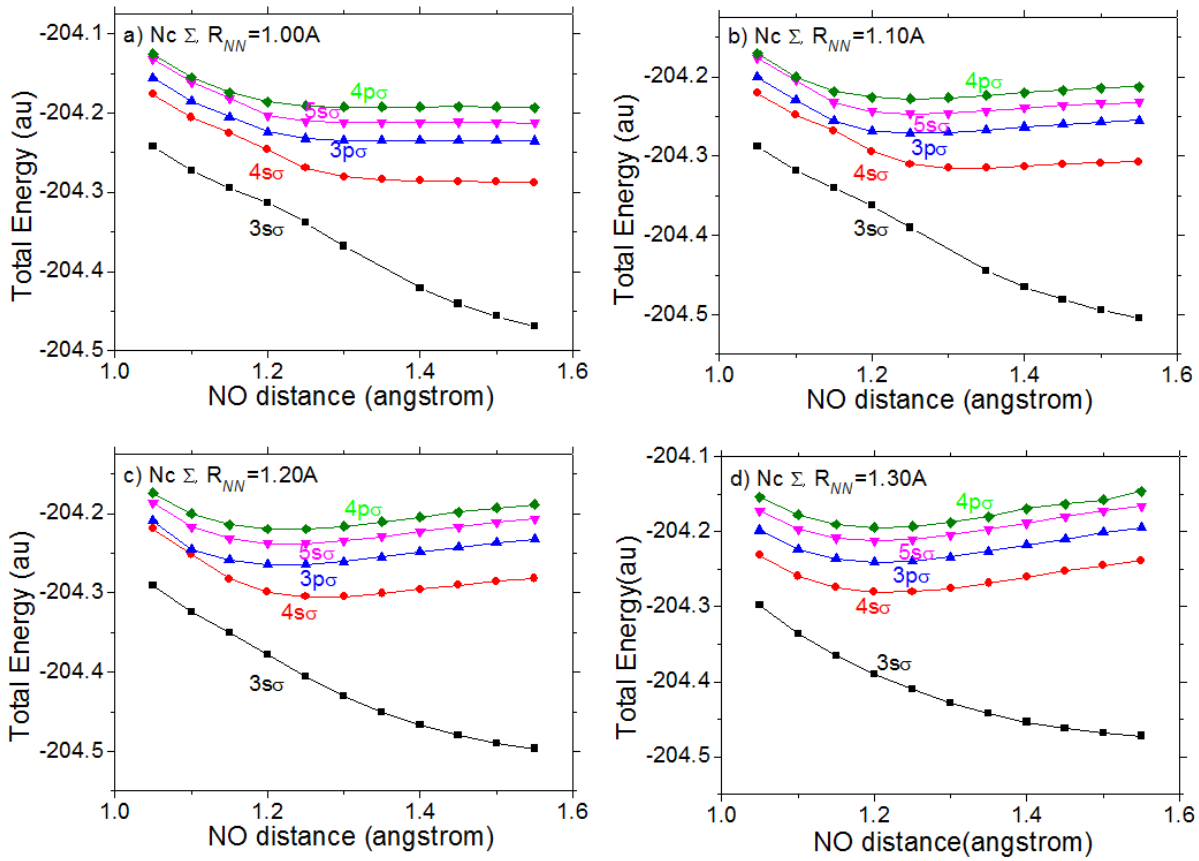

Figure 10. The 2D PESs of the low-lying N_c 1s excited states (nsσ (n = 3–5) and npσ (n = 3, 4) transitions) of N_2O in the R_{NO} coordinate for R_{NN} = 1.00, 1.10 [37], 1.20, and 1.30 Å.

Acknowledgments
The experiment was carried out with the approval of the SPring-8 program review committee. This study was supported by JST-CREST, a Grants-in-Aid for Scientific Research from the Japanese Society for the Promotion of Science (JSPS) and the Next Generation Supercomputing Project. The computations were partly performed at Research Center for Computational Science, Okazaki, Japan.

References
[1] Siegbahn K, Nordling C, Johansson G, Hdman J, Heden P F, Hamrin K, Gelius U, Bergmark T, Werme L O, Manne R and Baer Y 1969 *ESCA Applied to Free Molecules* (North-Holland, Amsterdam)
[2] Ueda K 2003 *J. Phys. B: At. Mol. Opt. Phys.* **36** R1
[3] Adachi J, Kosugi N, Shigemasa E and Yagishita A 1995 *J. Chem. Phys.* **102** 7369
[4] Tanaka T et al. 2006 *Chem. Phys. Lett.* **428** 34
[5] Prince K C, Avaldi L, Coreno M, Camilloni R and Simone M d 1999 *J. Phys. B:At. Mol. Opt. Phys.* **32** 2551
[6] Nakatsuji H 1973 *J. Am. Chem. Soc.* **95** 345

[7] Nakatsuji H and Koga T 1981 *The Force Concept in Chemistry* (Van Nostrand Reinhold Company, New York)
[8] Peyerimhoff S D 1975 *Adv. Quantum Chem.* **9** 69
[9] Buenker R J and Peyerimhoff S D 1968 *Theor. Chim. Acta* **12** 183
[10] Cederbaum L S and Domcke W 1977 *J. Chem. Phys.* **66** 5084
[11] Cederbaum L S, Domcke W, Schirmer J and von Niessen W 1986 *Adv. Chem. Phys.* **65** 115
[12] Nakatsuji H 1978 *Chem. Phys. Lett.* **59** 362
[13] Nakatsuji H 1979 *Chem. Phys. Lett.* **67** 329
[14] Jana D and Mukherjee D 2005 *J. Chem. Phys.* **122** 234101
[15] Nakata A, Tsuneda T and Hirao K 2009 *J. Comp. Chem.* **30** 2583
[16] Nakatsuji H 1992 *Acta Chim. Hungarica, Models in Chemistry* **129** 719
[17] Ehara M, Hasegawa J and Nakatsuji H 2005 *SAC-CI Method Applied to Molecular Spectroscopy, in Theory and Applications of Computational Chemistry: The First 40 Years, A Volume of Technical and Historical Perspectives* (Elsevier) p. 1099
[18] Nakatsuji H 1991 *Chem. Phys. Lett.* **177** 331
[19] Ehara M and Nakatsuji H 1998 *Chem. Phys. Lett.* **282** 347
[20] Fukuda R and Nakatsuji H 2008 *J. Chem. Phys.* **128** 094105
[21] Sankari R, Ehara M, Nakatsuji H, Senba Y, Hosokawa K, Yoshida H, Fanis A D, Tamenori Y, Aksela S and Ueda K 2003 *Chem. Phys. Lett.* **380** 647
[22] Kuramoto K, Ehara M and Nakatsuji H 2005 *J. Chem. Phys.* **122** 014304
[23] Ueda K, Hoshino M, Tanaka T, Kitajima M, Tanaka H, Fanis A D, Tamenori Y, Ehara M, Oyagi F, Kuramoto K and Nakatsuji H 2005 *Phys. Rev. Lett.* **94** 243004
[24] Ehara M, Nakatsuji H, Matsumoto M, Hatamoto T, Liu X-J, Lischke T, Pruemper G, Tanaka T, Makochekanwa C, Hoshino M, Tanaka H, Harries J R, Tamenori Y and Ueda K 2006 *J. Chem. Phys.* **124** 124311
[25] Ehara M, Kuramoto K, Nakatsuji H, Hoshino M, Tanaka T, Kitajima M, Tanaka H, Tamenori Y, Fanis A D and Ueda K 2006 *J. Chem. Phys.* **125** 114304
[26] Ehara M, Tamaki R, Nakatsuji H, Lucchese R R, Soderstrom J, Tanaka T, Hoshino M, Kitajima M, Tanaka H, Fanis A D and Ueda K 2007 *Chem. Phys. Lett.* **438** 14
[27] Ehara M and Nakatsuji H 2008 *Coll. Czech Chem. Commun.* **73** 771
[28] Tanaka T, Ueda K, Feifel R, Karlsson L, Tanaka H, Hoshino M, Kitajima M, Ehara M, Fukuda R, Tamaki R and Nakatsuji H 2007 *Chem. Phys. Lett.* **435** 182
[29] Tanaka T, Hoshino M, Kato H, Ehara M, Yamada N, Fukuda R, Nakatsuji H, Tamenori Y, Harries J R, Prumper G, Tanaka H and Ueda K 2008 *Phys. Rev. A* **77** 012709
[30] Dunning Jr. T H 1989 *J. Chem. Phys.* **90** 1007
[31] Kaufmann K, Nager C and Jungen M 1985 *Chem. Phys.* **95** 385
[32] Teffo J L and Chedin A 1989 *J. Mol. Spectrosc.* **135** 389
[33] Frisch M J et al 2010 Gaussian Development Version, Revision H. 06, Gaussian Inc., Wallingford CT.
[34] Lill J V, Parker G A and Light J C 1982 *Chem. Phys. Lett.* **89** 483
[35] Beck M H and Meyer H-D 2001 *J. Chem. Phys.* **114** 2036
[36] Worth G A, Beck M H, Jackle A and Meyer H-D 2003 *The MCTDH Package, Version 8.3, University Heidelberg,* Heidelberg, Germany
[37] Ehara M, Horikawa T, Fukuda R, Nakatsuji H, Tanaka T, Hoshino M, Tanaka H and Ueda K *submitted for publication*